Integration of contractile forces during tissue invagination

Adam C. Martin,[1] Michael Gelbart,[2,3] Rodrigo Fernandez-Gonzalez,[4] Matthias Kaschube,[2,3] and Eric F. Wieschaus[1]

[1]Department of Molecular Biology, Howard Hughes Medical Institute, [2]Lewis-Sigler Institute for Integrative Genomics, and [3]Joseph Henry Laboratories of Physics, Princeton University, Princeton, NJ 08544
[4]Developmental Biology Program, Sloan-Kettering Institute, New York, NY 10065

Contractile forces generated by the actomyosin cytoskeleton within individual cells collectively generate tissue-level force during epithelial morphogenesis. During *Drosophila* mesoderm invagination, pulsed actomyosin meshwork contractions and a ratchet-like stabilization of cell shape drive apical constriction. Here, we investigate how contractile forces are integrated across the tissue. Reducing adherens junction (AJ) levels or ablating actomyosin meshworks causes tissue-wide epithelial tears, which release tension that is predominantly oriented along the anterior–posterior (a-p) embryonic axis.

Epithelial tears allow cells normally elongated along the a-p axis to constrict isotropically, which suggests that apical constriction generates anisotropic epithelial tension that feeds back to control cell shape. Epithelial tension requires the transcription factor Twist, which stabilizes apical myosin II, promoting the formation of a supracellular actomyosin meshwork in which radial actomyosin fibers are joined end-to-end at spot AJs. Thus, pulsed actomyosin contractions require a supracellular, tensile meshwork to transmit cellular forces to the tissue level during morphogenesis.

Introduction

Throughout development, epithelial sheets of cells undergo dramatic rearrangements, such as tissue folding and invagination, to generate complex three-dimensional organs in a process called epithelial morphogenesis (Leptin, 2005; Lecuit and Lenne, 2007; Quintin et al., 2008). Epithelial morphogenesis results from coordinated cell shape changes and movements that collectively deform tissues (Holtfreter, 1943; Gustafson and Wolpert, 1962; Sweeton et al., 1991; Shih and Keller, 1992). Individual cell shape changes and movements require that forces are generated within cells. In addition, for cellular forces to result in coherent changes in tissue architecture, forces must be transmitted between epithelial cells. The mechanical coupling of epithelial cells implies that the integration of cellular forces can in turn influence individual cell dynamics (Peralta et al., 2007; Gorfinkiel et al., 2009; Pouille et al., 2009; Solon et al., 2009). Therefore, understanding tissue morphogenesis requires determining how cellular forces are integrated across tissues and whether tissue-level forces feed back to control individual cell behaviors.

A common cell shape change that results in epithelial morphogenesis is apical constriction. Apical constriction reduces the apical cross-sectional area of an epithelial cell, which transforms a columnar cell to a wedge or cone shape. Coordinated apical constriction of mechanically coupled cells promotes epithelial folding and tissue invagination (Odell et al., 1981). During *Drosophila* gastrulation, apical constriction appears to be required for the invagination of the prospective mesoderm, a strip of ~1,200 cells along the ventral midline of the embryo (Leptin and Grunewald, 1990; Parks and Wieschaus, 1991; Sweeton et al., 1991). Apical constriction of mesoderm cells is polarized, or anisotropic, such that cells constrict predominantly in the ventral–lateral (v-l) direction, remaining longer along the anterior–posterior (a-p) axis (Fig. 1 A; Sweeton et al., 1991). The mechanism responsible for anisotropic constriction is not known, but one consequence is that whereas the tissue contracts in the v-l direction, a-p tissue length remains relatively constant, resulting in a long, narrow ventral furrow.
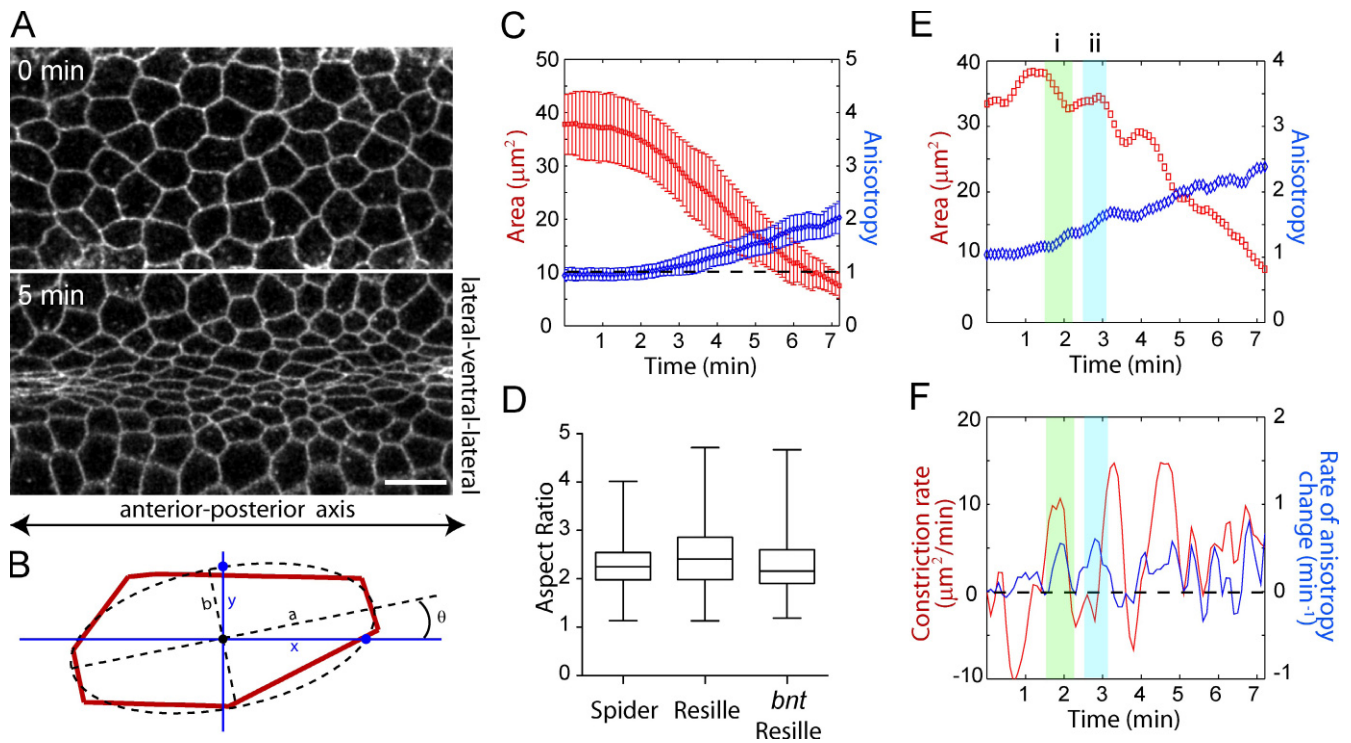
Figure 1.   **Polarized apical constriction possibly reflects tissue mechanics.** (A) Images of ventral furrow cell outlines in a live embryo using Spider-GFP. Bar, 10 μm. (B) Schematic showing the method used to calculate the aspect ratio (a/b) and anisotropy (x/y) of a cell. (C) Mean cross-sectional area (red) and anisotropy (blue) over time for a single embryo. Error bars indicate SD (n = 42 cells). The broken line marks an anisotropy of 1 (isotropic). (D) Box and whisker plot of aspect ratios from Spider-GFP, Resille-GFP, and *bicoid nanos torso-like* (*bnt*) Resille-GFP embryos. Boxes extend from to 25th to 75th percentile, with a line at the median. Whiskers extend to the most extreme values. Each sample represents three embryos, with 123, 102, and 158 cells. (E and F) Apical area and anisotropy (E) or constriction rate and the time derivative of anisotropy (F) for an individual cell over time. Anisotropy increases both during (i) and between (ii) contraction pulses. The broken line marks a rate of 0.

Understanding the cause of anisotropy requires elucidating the mechanisms of force generation in cells and tissues. In ventral furrow cells, apical constriction is driven by pulsed contractions of an actomyosin meshwork that spans the apical cortex and is coupled to the cell surface via adherens junctions (AJs; Dawes-Hoang et al., 2005; Martin et al., 2009; Sawyer et al., 2009). Between contractions, the constricted state of the cell is stabilized such that cells constrict incrementally via a ratchet-like mechanism (Martin et al., 2009). Anisotropic constriction in ventral furrow cells could thus result from an individual cell's behavior if, for example, force generation during contraction pulses was directional.

Alternatively, anisotropic constriction could reflect mechanical constraints on individual cell constriction imposed by the mechanical properties of the tissue (Hardin and Keller, 1988), such as greater tension along the a-p axis. Actomyosin contractility associated with apical constriction likely generates epithelial tension; however, it is unclear how tension is directed across the mesoderm primordium. Furthermore, how pulsatile and stable contractile forces contribute to the global mechanical properties of the tissue is unknown. In this study, we combine live imaging, computational image analysis, laser ablation, and genetics to examine the influence of tissue mechanics on individual cell shape changes and the mechanisms by which cellular forces are transmitted across the tissue.

Results

Anisotropic apical constriction possibly reflects tissue mechanics

Polarized constriction could result from an individual cell behavior, such as directional actomyosin-based force generation along the v-l axis. Alternatively, a mechanical property of the tissue, such as greater tension along the a-p axis, could bias the direction in which cells constrict. Because ventral furrow cell apical constriction is pulsed (Martin et al., 2009), we decided to distinguish between these possibilities by determining whether the increase in cell polarization correlates with pulses of actomyosin contraction in individual cells. To visualize apical cell shape, we imaged ventral furrow cells in live embryos expressing the membrane markers Spider-GFP and Resille-GFP (Morin et al., 2001). We quantified the polarization of apical constriction by fitting apical cell outlines with ellipses and measuring two parameters (Fig. 1 B). Cell aspect ratio, which is independent of the orientation to the a-p axis (Fig. 1 B, θ), was measured by dividing the major axis of the fitted ellipse (a) by the minor axis (b). In addition, we measured cell "anisotropy" relative to the embryonic axis by dividing the cell's length along the a-p axis (Fig. 1 B, x) by the cell's length along the v-l axis (y). Aspect ratio and anisotropy had similar values in elongated cells during furrow formation because cells were aligned along the a-p axis such that θ was ~0 (unpublished data).

Mean anisotropy and aspect ratio gradually increased to ∼2 before cells invaginated into the embryo interior (Fig. 1, C and D). Analysis of individual cells demonstrated that transient increases in anisotropy did sometimes coincide with contraction pulses (Fig. 1, E and F, i). However, anisotropy also increased between contractions (Fig. 1, E and F, ii). Overall, there was not a strong correlation between the constriction rate and the rate of change in anisotropy (r = 0.1 ± 0.24, n = 125 cells, three embryos), which suggests that directional contraction of individual cells is not solely responsible for the anisotropy. Furthermore, anisotropic constriction still occurred in *bicoid nanos torso-like* (*bnt*) embryos that lack a-p polarity, which demonstrates that directional information for individual cell constriction is not provided by the a-p patterning system (Fig. 1 D). These results suggest that rather than being caused by discrete cellular behaviors, anisotropic apical constriction could result from the global mechanics of the tissue.

AJs integrate contractile forces to generate epithelial tension

AJs, which contain complexes of the transmembrane adhesion molecule E-cadherin and the adaptors β-catenin and α-catenin, link neighboring cells to each other and link the cell surface to the actin cortex (Gumbiner, 2005). Partial loss-of-function mutants in the *Drosophila* β-catenin (Armadillo [Arm]), such as arm^{043A01}, result in lower levels of Arm, E-cadherin, and α-catenin at the cell surface (Cox et al., 1996; Sokac and Wieschaus, 2008; Sawyer et al., 2009). Therefore, to determine whether there are mechanical properties of the ventral furrow that might explain cell anisotropy, we examined the consequences of reducing AJ levels using maternal and zygotic arm^{043A01} mutants ($arm^{M/Z}$). Because contractile forces for apical constriction are generated by myosin II on the apical surface, we first visualized apical myosin-GFP in live $arm^{M/Z}$ embryos. In wild-type embryos, myosin II forms a meshwork on the ventral surface of the embryo (Fig. 2 A and Video 1; Martin et al., 2009). In some $arm^{M/Z}$ embryos (n = 4/11), myosin II structures uniformly dissociated across the tissue, presumably because of the global lack of cell adhesion (unpublished data). However, in the majority of $arm^{M/Z}$ embryos (n = 7/11), the myosin II meshwork remained locally intact, but tore across the entire width of the ventral furrow at apparently random positions along the a-p axis before completely dissociating (Fig. 2 A and Video 1). Myosin-GFP in the adjacent tissue retracted away from the tear, widening the gap in the myosin II meshwork (Fig. 2 B). Epithelial tears occurred in the ventral furrow but were not observed in more lateral ectoderm at the same stage (unpublished data). These results suggest that apical constriction of ventral furrow cells generates epithelial tension, which can disrupt cell–cell adhesion in embryos with weakened AJs. Similar epithelial tears and tissue retractions were observed when *arm* (23/24 *armRNAi* embryos), E-cadherin (10/12 *ECad2RNAi* embryos), or α-catenin (3/12 *α-cateninRNAi* embryos) expression was knocked down using RNAi, which demonstrates that all core AJ components are required for epithelial tension

(Fig. S1, A and B). However, the most striking feature of these tears was that the associated tissue retraction was always directed along the a-p axis of the embryo. This suggests that epithelial tension transmitted through AJs is highest along the a-p axis during ventral furrow formation, which could explain the observed cell anisotropy.

Epithelial tension is highest along the length of the ventral furrow

It was possible that decreasing the levels of AJ proteins changed the wild-type distribution of tensile forces present in the mesoderm primordium. Therefore, we sought to test whether tension is anisotropic in this tissue by using an independent approach. Laser ablation has served as an excellent method to measure relative tensile forces in epithelial tissues undergoing morphogenesis (Kiehart et al., 2000). Targeted UV laser irradiation severs actin- and myosin II–containing structures, resulting in the recoil of the surrounding tissue whose initial velocity (displacement/time) immediately after ablation is proportional to the magnitude of the resting tension (Hutson et al., 2003; Fernandez-Gonzalez et al., 2009). Because tissue retraction associated with local ablations could be influenced by the orientation of cellular actomyosin structures, we first made 20-μm-long multicellular laser incisions along either the a-p or v-l axes and measured the initial myosin II displacement perpendicular to the incision at various distances from the incision (Fig. 3 A). Incisions across the width of the ventral furrow resulted in dramatic myosin displacement all along the a-p axis of the embryo (D_{ap}), which indicates tension along this axis (Fig. 3 B and Video 2). Laser incisions parallel to the furrow resulted in significantly less displacement along the v-l axis (D_{vl}; Fig. 3 B and Video 2), which is consistent with there being lower v-l tension. To more accurately measure the initial velocity of tissue retraction, we also performed 1-μm point ablations in which we imaged myosin II displacement within 3 s of initiating ablation (compared with 9 s for line ablation, Fig. S2). Ablation of isometric-looking myosin structures resulted in retraction of the surrounding tissue (Fig. 3 D). To determine if this displacement was directional, we measured the initial radial displacement of myosin structures (D_r) from the site of ablation at different angles (θ) representing different directions relative to the a-p and v-l axes (Fig. 3 E). The initial radial displacement in wild-type embryos was 2–3-fold higher along the a-p axis of the embryo (Fig. 3 F). These results confirm the conclusions from our analysis of $arm^{M/Z}$ mutants and demonstrate that epithelial tension is predominantly directed along the length of the ventral furrow.

Epithelial tension along the a-p axis causes anisotropic apical constriction

The higher tension along the a-p axis suggests the possibility that ventral furrow cells attempt to constrict isotropically, but encounter more resistance and thus constrict less along the a-p axis. To determine whether epithelial tension biases constriction to occur in the v-l direction, we examined how the disruption of epithelial tension that results from AJ depletion affects cell shape change in both live and fixed embryos.
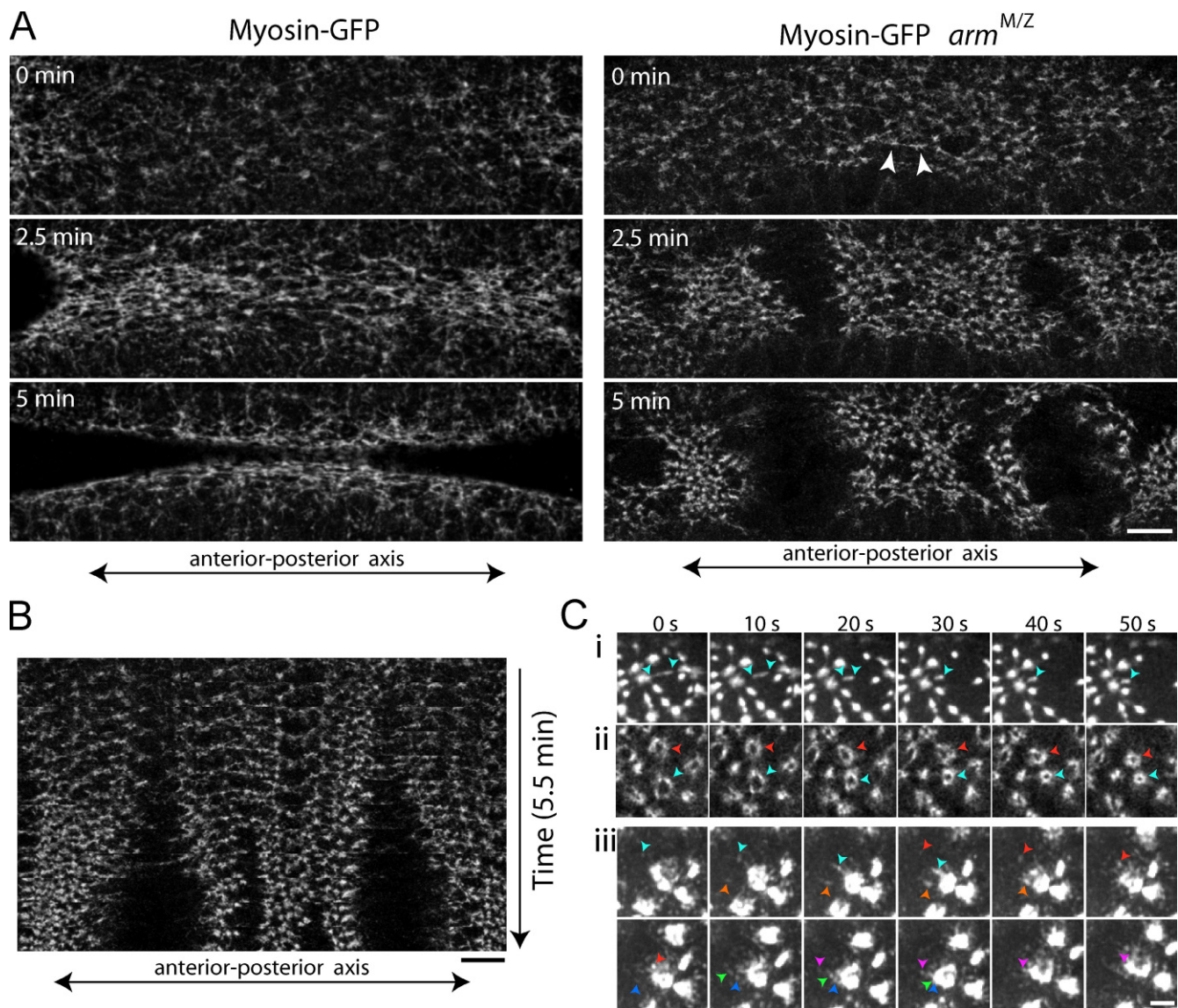
Figure 2. **AJs integrate global epithelial tension.** (A) Myosin II in live wild-type or $arm^{M/Z}$ embryos. Myosin II initially starts to form a meshwork in $arm^{M/Z}$ (arrowheads), but the meshwork separates at discrete positions along the a-p axis. (B) Kymograph of actomyosin meshwork separation in an $arm^{M/Z}$ embryo. (C) Tearing of the supracellular meshwork alters myosin II organization and dynamics. Myosin II fibers that normally extend between myosin II spots retract (blue arrows) in $arm^{M/Z}$ embryos (i). Loss of cell adhesion in $armRNAi$ embryos causes myosin II to form rings (red and blue arrows) that contract (ii). Contracted myosin II rings in $armRNAi$ embryos exhibit continuous, unrestrained cortical flow of myosin II spots (colored arrows track myosin spots over time) into the ring (iii). Bars: (A) 10 µm; (B) 10 µm; (C) 5 µm.

In $armRNAi$ embryos, cells within the tear rapidly expanded after dissociation of myosin II structures (Fig. 4, A and B; and Video 3). These distended cells abnormally changed neighbors as they expanded, which suggests that they had lost adhesion to one another (Fig. 4 C). Simultaneous with local cell expansion in the tear, the surrounding cells appeared to lose their a-p polarization and underwent isotropic apical constriction (Fig. 4, A and D; and Video 3). In live $armRNAi$ embryos, cells that constricted after a neighboring epithelial tear exhibited a mean anisotropy of 1.07 ± 0.27 (mean $\pm$ SD, $n = 120$ cells, three embryos), which is close to being perfectly isotropic (anisotropy = 1). Furthermore, we observed cases in live $armRNAi$ and $ECad2RNAi$ embryos where cells began to constrict anisotropically and then became more isotropic after

epithelial tearing events (Fig. 4, D, E, and F). These results strongly suggest that individual cells are not hard-wired to undergo polarized contraction, but that apical constriction generates higher epithelial tension along the a-p axis, providing a mechanical constraint that feeds back to control the resulting individual cell shape.

Actomyosin fibers connected by spot AJs form a supracellular meshwork

We next examined how contractile forces are transmitted across the tissue. The epithelial tears in $arm^{M/Z}$ embryos suggested that apical actomyosin meshworks are coupled to each other through AJs. Therefore, we examined how cytoskeletal structures are linked between cells during ventral furrow formation
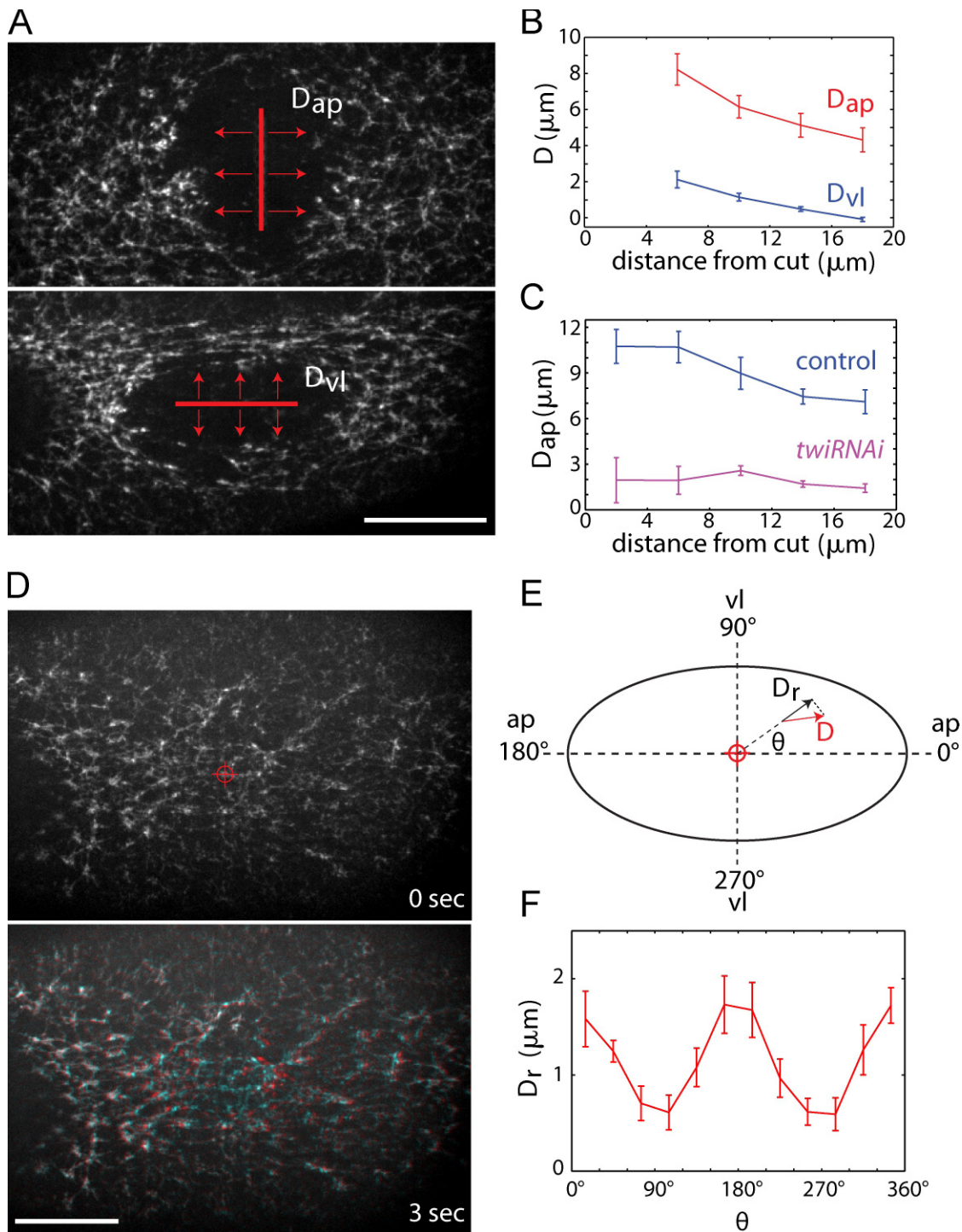
Figure 3. **Epithelial tension is highest along the length of the furrow.** (A) Myosin-GFP images immediately after laser incisions (red lines, 20 μm) were made perpendicular to (top) or parallel to (bottom) the furrow. Myosin displacements perpendicular to these incisions (D_{ap} and D_{vl}) were measured. Bar, 20 μm. (B) D_{ap} and D_{vl} as a function of distance from the laser incision. The data were grouped into 4-μm bins (0–4, 4–8, etc...) and data points are mean ± SEM (indicated by error bars; $n = 4$ embryos). (C) D_{ap} as a function of distance for H_2O-injected (control) and twiRNAi embryos. Data points are the same as in B ($n = 5$ embryos). (D) Myosin-GFP images before (top) and after (bottom) a point ablation (crosshair). In the bottom panel, the post-ablation image (red) overlays the pre-ablation image (blue) to illustrate myosin displacement. Bar, 20 μm. (E) Schematic illustrating the method used for quantifying radial myosin displacement (D_r) in the direction (θ) relative to the a-p and v-l axes. Radial displacement is the component of the measured displacement (D) along direction θ. (F) D_r as a function of θ. The data were grouped into bins of 30° and data points are mean ± SEM (indicated by error bars; $n = 5$ embryos).

using fixed embryos labeled with myosin II, actin, and E-cadherin. Before furrow formation, the majority of myosin II was present as isolated spots on the apical surface of individual cells,

the largest of which likely resulted from pulses of myosin II coalescence (Fig. 5 A). As myosin II levels increased and a furrow developed, myosin II and actin formed supracellular

Figure 4. **Anisotropic apical constriction results from a-p epithelial tension.** (A and B) Apical myosin II (green) and subapical F-actin used to visualize cell outlines (white) in fixed *armRNAi* embryos. (A) A tear similar to those observed in live embryos. Red arrows indicate cells that have constricted isotropically. (B) A later-staged embryo where myosin II has rounded up into rings. (C) Disruption of AJs results in loss of cell–cell adhesion. Time-lapse images of cell outlines (Spider-GFP) during a tear in an *armRNAi* embryo. Red cell–cell contacts are lost and different cells come into contact (blue). (D) Isotropic apical constriction occurs upon tearing. Time-lapse images of cell outlines (Spider-GFP) in an *E-CadherinRNAi* embryo. Blue dots indicate initially anisotropic cells that constrict isotropically upon loss of epithelial integrity. Apical area (E) and anisotropy (F) were quantified for the cells labeled in D. Dotted lines indicates the time of the tear. Bars: (A and B) 10 µm; (C) 5 µm; (D) 5 µm.
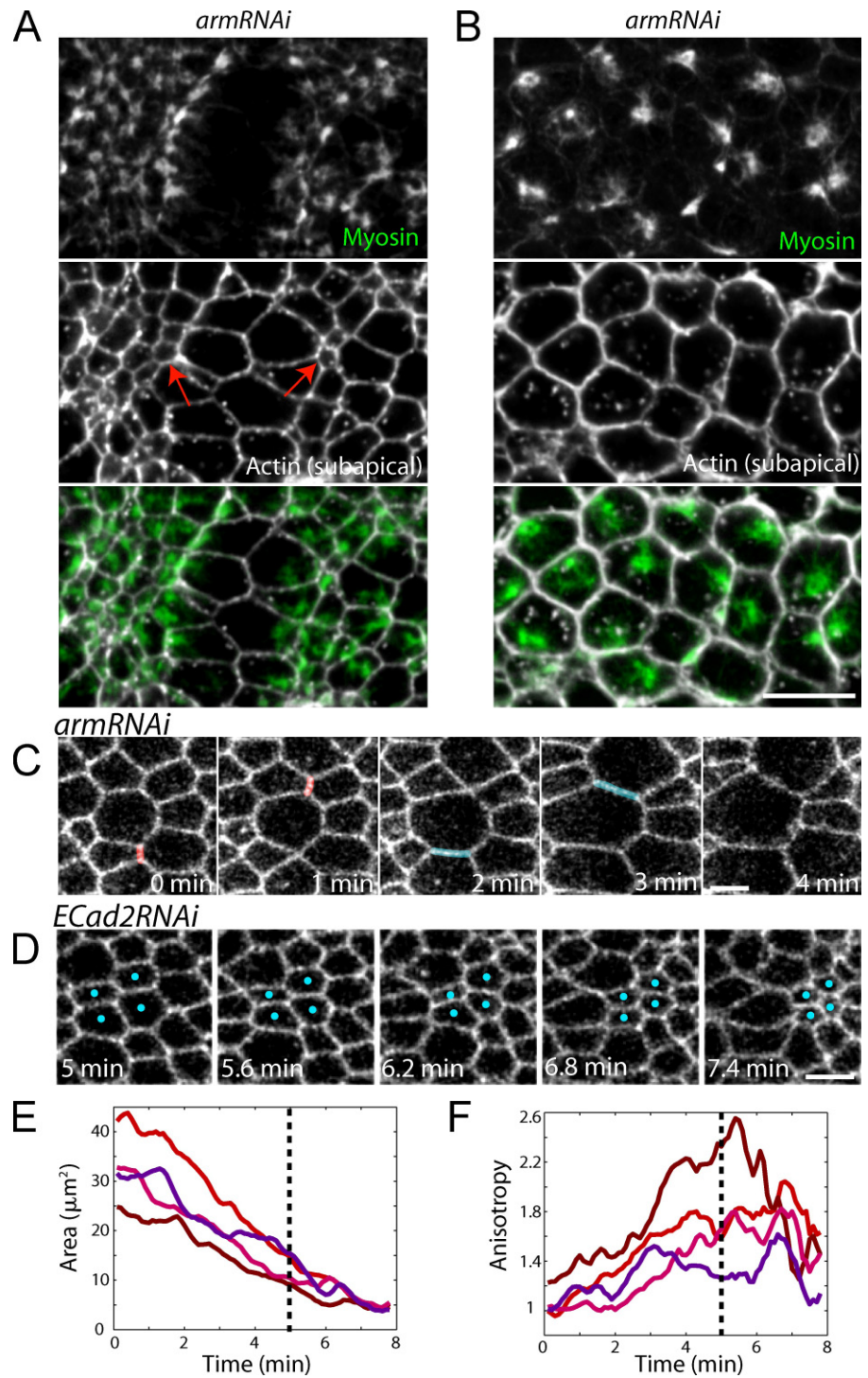
fibers that extended across multiple cells and were incorporated into the tissue-wide meshwork (Fig. 5, A and B). Supracellular actomyosin fibers bridged the apical surface of the cell, such that the ends of myosin II fibers met at cell–cell interfaces (Fig. 5 B, i). Multiple radial actomyosin fibers often originated from a central myosin II spot or ring, which formed branches in the tissue-wide meshwork (Fig. 5 B, i). In addition to radial actomyosin fibers, some supracellular actomyosin fibers ran along cell boundaries (Fig. 5 B, ii). In ventral furrow cells, subapical AJs ~4 µm below the apical cortex are dis-

assembled and reappear at the apical surface as spotlike structures between cell vertices (Fig. 5 C; Dawes-Hoang et al., 2005; Kölsch et al., 2007; Martin et al., 2009). Spot AJs appeared to connect radial actomyosin fibers end-to-end to generate the supracellular fibers (Fig. 5 C). Interestingly, spot AJs linking actomyosin fibers were often stretched along the fiber, possibly indicating tension being exerted on the junction (Fig. 5 C). Thus, spot AJs appear to integrate cellular actomyosin networks into supracellular actomyosin fibers, resulting in a tissue-wide actomyosin meshwork.
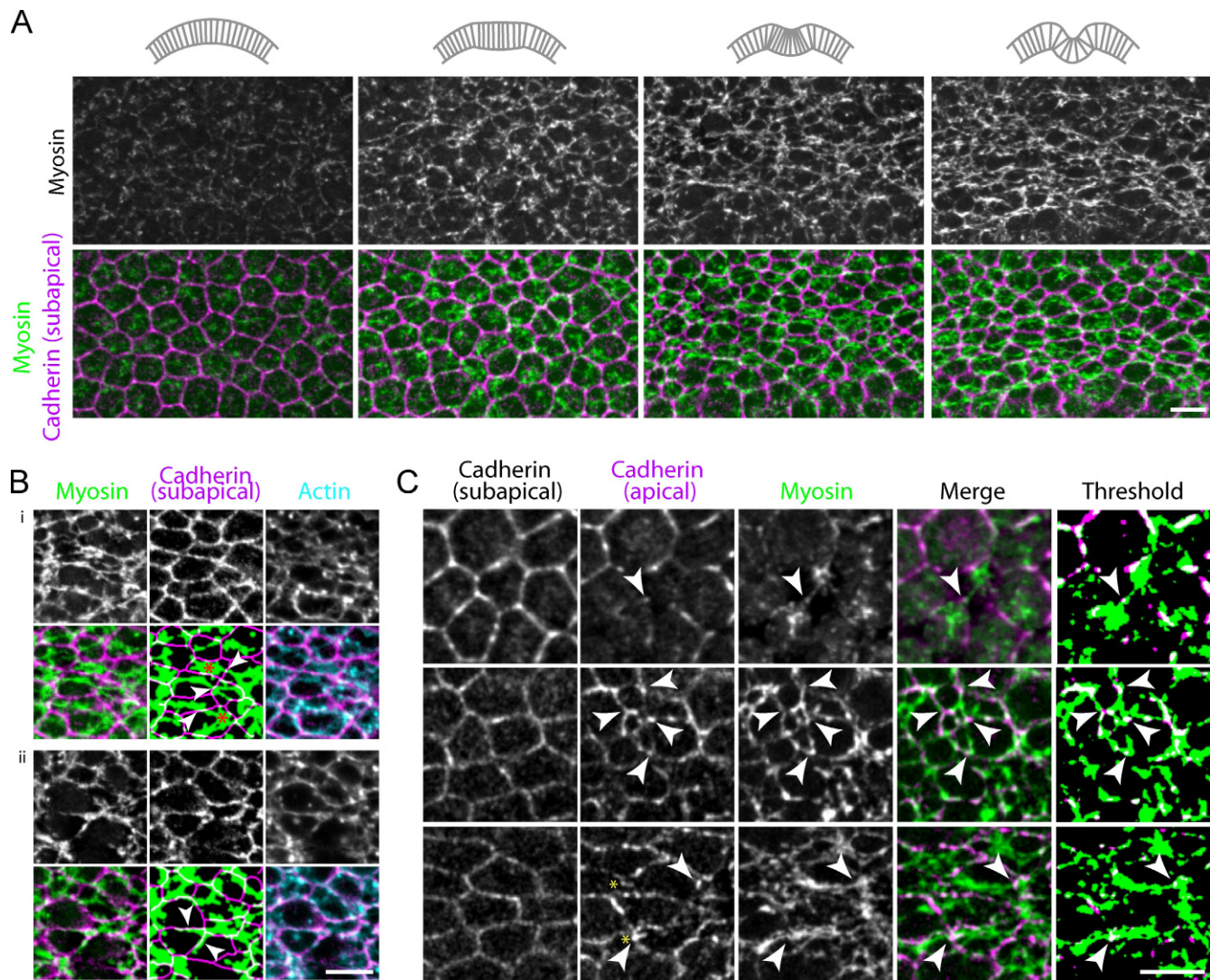
Figure 5. **Spot AJs integrate actomyosin fibers to form a supracellular meshwork.** (A) Apical myosin II (green) and subapical E-cadherin, ∼2 µm below the apical cortex (purple), in fixed embryos. Schematics indicating the stage of furrow formation are shown above each image pair. (B) Magnified view of supracellular actomyosin fibers. Apical myosin II (green), subapical E-cadherin (purple), and apical actin filaments (cyan) were imaged in fixed embryos. Supracellular actomyosin fibers are often oriented perpendicular to cell interfaces (i, arrows), but can also be seen running parallel to cell interfaces (ii, arrows). Actomyosin fibers often radiated from a central myosin II spot or ring (red asterisks). The bottom-middle images of i and ii were thresholded to facilitate visualization of myosin II fibers. (C) Apical E-cadherin (purple) and myosin II (green) in fixed embryos. Subapical E-cadherin staining is used to illustrate cell outlines. Myosin II fibers connect to apical E-cadherin puncta, or spot AJs (arrows). In late stages, spot AJs can appear stretched along the fiber (yellow asterisks). Bars, 5 µm.

Spot AJs transmit tension from actomyosin fibers across the plasma membrane

To test whether spot AJs transmit tension between cellular actomyosin fibers, we examined more closely the cellular organization and dynamics of myosin II in embryos with reduced AJs. Supracellular actomyosin fibers initially formed in $arm^{M/Z}$ embryos, which is consistent with this allele retaining partial function (Fig. 2 A). However, upon epithelial tearing, myosin II fibers rapidly contracted, demonstrating that myosin II fibers generate contractile force in a manner similar to stress fibers (Fig. 2 C, i; and Video 4; Kumar et al., 2006). Loss of cell adhesion resulted in myosin II contraction into rings or balls across the entire epithelium (Fig. 2, A and C, ii and iii; and Fig. 4, A and B). Myosin II spots continuously flowed into myosin II

rings, suggesting that unrestrained actomyosin contraction occurs in the absence of opposing contractile forces from surrounding cells (Fig. 2 C, iii; and Video 5). These results suggest that spot AJs balance tensile forces generated by cellular actomyosin networks to allow the formation of stable actomyosin fibers that transmit tension across the tissue.

The retraction of actomyosin fibers in embryos with reduced AJs could reflect a disruption of the extracellular linkage between adjacent cell plasma membranes or the intracellular connection between the plasma membrane and the actomyosin cortex. To distinguish between these models, we examined whether cell membranes completely separate during tearing events using scanning EM. In the ventral furrow of wild-type embryos, boundaries between cells cannot be discerned because of tight adhesion of these cells through apical AJs (Fig. 6 A). In contrast, individual
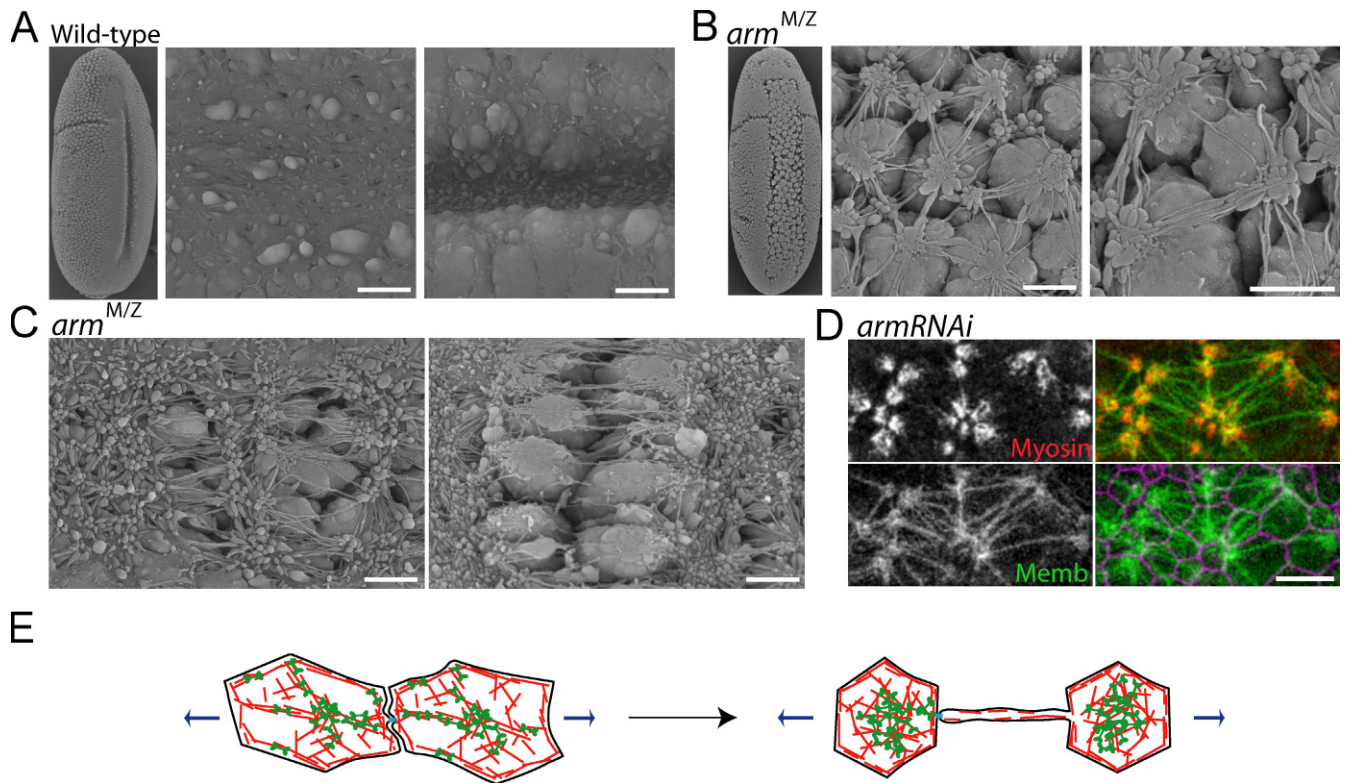
Figure 6. **Sensitizing AJs disrupts intracellular connections between the actomyosin cytoskeleton and the plasma membrane.** (A) Scanning EM of ventral furrows in wild-type embryos. (B and C) Scanning EM of *arm*$^{M/Z}$ embryos. Membrane tethers extend between dissociated cells (B) and across epithelial tears (C). (D) Myosin II localizes to regions of membrane blebs that are interconnected by membrane tethers. Images of apical myosin II (red, myosin-mCherry), apical membrane (green, Spider-GFP), and subapical membrane (purple) in live *armRNAi* embryos. (E) Model: Lower adhesion in *arm* mutants causes higher tension per adhesive structure, leading to the rupture of fiber–AJ connections. Bars: (A–C) 5 µm; (D) 10 µm.

ventral cells can easily be identified in *arm*$^{M/Z}$ mutants because cells lose tight adhesion to one another, specifically in the ventral furrow region (Fig. 6 B). In addition, we identified tearing events in which adjacent rows of cells became separated (Fig. 6 C). Scanning EM demonstrated that the cell expansion observed using confocal microscopy represented cells rounding up upon loss of adhesion. Consistent with the global contraction of the surrounding tissue in live embryos, the isotropically constricting cells adjacent to the tear contained dramatic membrane blebs, which suggests that the apical cortex rapidly contracts upon loss of epithelial tension across the tissue.

Despite the dramatic loss of adhesion, cells in *arm*$^{M/Z}$ embryos maintained thin membrane connections, or tethers, to their neighbors (Fig. 6, B and C). Live imaging of the apical surface during tearing events demonstrated that membrane tethers form as cell apices contract away from each other (Video 6). Membrane tethers remained connected to clusters of membrane blebs, which colocalized with myosin II rings and some remaining cortical E-cadherin (Figs. 6 D and S1 C). Tethers often contained detectable levels of F-actin, but not myosin II, which suggests that tethers fail to transmit tension (Fig. S1 D). We propose that membrane tethers form when the actomyosin cortex detaches from the one side of a fiber–AJ–fiber connection (Fig. 6 E). This detachment did not indicate a specific function for β-catenin in coupling the actomyosin cortex to AJs because membrane tethers were also observed in both *α-cateninRNAi*

and *ECad2RNAi* embryos (Fig. S1 E). Thus, reducing the number of AJs possibly focuses the large amount of contractile force generated by ventral furrow cells onto the few remaining AJ–cytoskeleton connections, exceeding the forces of adhesion and causing junctions to detach from the tensile meshwork. However, because we have been unable to completely disrupt AJs, we cannot rule out the possibility that membrane tethers result from cell–cell adhesion that is E-cadherin and Arm independent. Regardless of the exact nature of the membrane connection, tether formation upon disruption of AJs further argues that spot AJs balance contractile forces across the plasma membrane, allowing tension to be transmitted between cells.

Epithelial tears and loss of cell–cell adhesion fail to occur in the absence of Snail-mediated actomyosin contraction

We have hypothesized that the epithelial tears observed in embryos with disrupted AJs result from contractility of the supracellular actomyosin meshwork. We previously showed that the transcription factor Snail is required for pulsed contractions and apical actomyosin meshwork assembly (Martin et al., 2009). Therefore, we determined whether Snail is required for the epithelial tears and loss of cell adhesion observed in *arm* mutant embryos by performing double RNAi experiments in which the expression of *sna* was reduced in combination with *arm*. A control double-stranded RNA (dsRNA; *CG3651RNAi*) had no
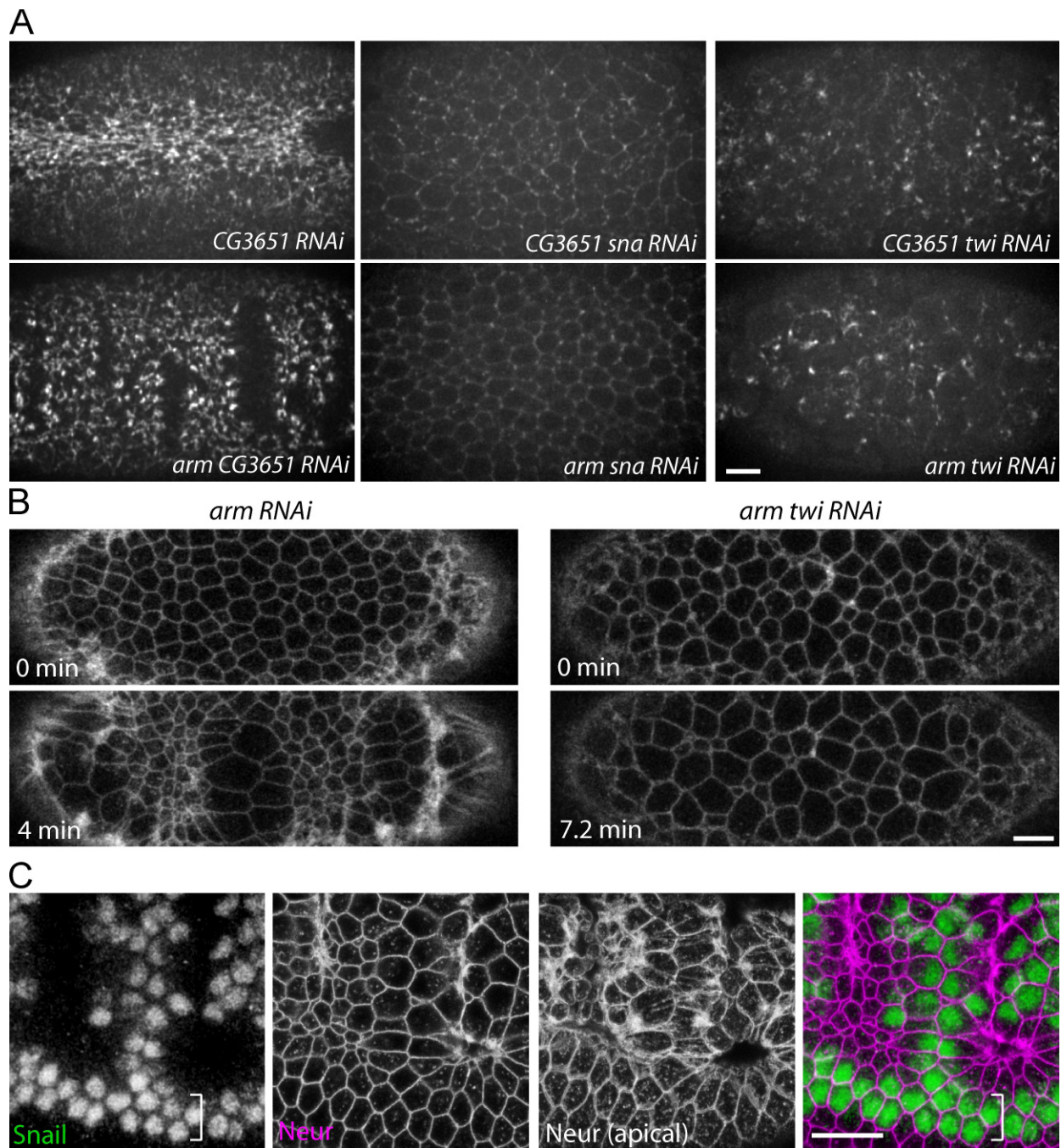
Figure 7. **Snail and Twist are required for epithelial tearing.** (A) Images of myosin-GFP in live embryos injected with the indicated dsRNA. *snaRNAi* inhibits the formation of myosin II rings and the loss of cell–cell adhesion normally observed in *armRNAi* embryos. *twiRNAi* inhibits tearing, but myosin contractions still occur. (B) Images of cell outlines (Spider-GFP) in *armRNAi* and *arm-twiRNAi* embryos. Knockdown of Twist suppresses the formation of discrete epithelial tears. (C) Epithelial tears and loss of cell–cell adhesion occur within the Snail expression domain. Images of a fixed *arm*$^{M/Z}$ embryo stained for Snail (green) and neurotactin (purple, cell outlines). An apical image of neurotactin is included to illustrate the position of the tear. The ventral midline is offset to visualize the lateral border of the mesoderm where two Snail-expressing nuclei do not initially lose adhesion (white bracket). Bars, 10 μm.

effect on its own or with *armRNAi* (Fig. 7 A and Video 7), which demonstrates that multiple dsRNAs can be combined without affecting the potency of RNAi. Knockdown of *sna* and *arm* suppressed the formation of epithelial tears and the loss of adhesion normally observed in *armRNAi* embryos (*n* = 5 embryos; Fig. 7 A and Video 8). In addition, *snaRNAi* suppressed apical myosin II recruitment and contraction into rings in *armRNAi* embryos. Thus, epithelial tearing and loss of cell adhesion fail

to occur in the absence of Snail-mediated actomyosin assembly, supporting the model that tension generated by the actomyosin contraction is responsible for these phenotypes.

Twist-mediated stabilization is required to transmit epithelial tension

The transcription factor Twist affects actomyosin contractility in the ventral furrow differently than Snail. Pulses of actomyosin

contraction still occur in *twi* mutant and *twiRNAi* embryos. However, the resulting constriction fails to be stabilized, possibly because of a defect in maintaining cortical tension (Martin et al., 2009). Therefore, we examined whether Twist is required for the epithelial tears in *armRNAi* embryos to distinguish the roles of pulsed actomyosin contraction and Twist-dependent stabilization in generating tissue-wide epithelial tension. Pulses of myosin II coalescence occurred in *twi-armRNAi* embryos, similar to *twiRNAi* alone (Fig. 7 A and Video 9). Similar to *armRNAi* embryos, cells lost adhesion and formed tethers and dramatic blebs in *twi-armRNAi* embryos (Figs. 7 B and S1 F). Thus, pulsed contractions generate local tension that can disrupt cell–cell adhesion. Pulses continued even after cells lost adhesion, which suggests that the pulsed contraction does not require mechanical interactions between cells. Importantly, cell dissociation occurred without the formation of tissue-wide tears along the a-p axis of the embryo (*n* = 10 embryos; Fig. 7, A and B; and Videos 9 and 10), which suggests that pulsed actomyosin contractions are insufficient to generate global epithelial tension. To further examine Twist's role in generating tension, we performed laser incisions across the width of the furrow and measured a-p myosin displacement (D_{ap}) in control (H_2O-injected) and *twiRNAi* embryos. *twiRNAi* embryos exhibited significantly lower levels of recoil at all distances from the incision, demonstrating that Twist is indeed required to transmit tension between ventral furrow cells (Fig. 3 C). Because Twist enhances Snail expression, it was possible that the disruption of epithelial tension was caused by lower levels of Snail activity (Kosman et al., 1991; Leptin, 1991). However, knockdown of the two Twist targets, *fog* and *t48* (Costa et al., 1994; Kölsch et al., 2007), also suppressed the formation of tissue-wide epithelial tears in *fog-t48-armRNAi* embryos, demonstrating that this Twist activity is independent of Snail (unpublished data). Consistent with the importance of Twist in generating tissue-wide tears, epithelial tears in *arm^{M/Z}* mutants are restricted to ~14 cells within the 18 cell–wide Snail expression domain (Fig. 7 C), corresponding to the domain of highest Twist expression, where transcriptional targets such as *folded gastrulation* are activated (Leptin, 1991; Costa et al., 1994). Thus, Twist-mediated stabilization is required to transmit tension across the tissue, which is required for epithelial tears in *arm* mutant embryos.

Twist stabilizes apical myosin II fibers between contraction pulses to form a supracellular actomyosin meshwork

Why do pulsed myosin II contractions in *twiRNAi* embryos fail to transmit tension across the tissue? To address this question, we used myosin-GFP and membrane-mCherry to compare cellular myosin II dynamics in wild-type and *twiRNAi* embryos. In wild-type cells, myosin II fibers remain on the apical cortex after contraction pulses during the stabilization phase of apical constriction (Fig. 8 A; Martin et al., 2009). This results in a gradual increase in cortical myosin II levels over a series of contractions (Fig. 8 B). In contrast, myosin II seemed to disappear from the apical cortex after contraction pulses in *twiRNAi* embryos, with myosin II levels falling back to near the same level

as before the pulse (Fig. 8, A and B). To determine whether *twiRNAi* affects cortical myosin II levels after contraction, we averaged normalized myosin II intensity profiles for individual pulses in control (*CG3651RNAi*) and *twiRNAi* embryos. We found that mean cortical myosin II intensity in *twiRNAi* embryos dropped to a significantly lower level after a contraction pulse than control embryos (Fig. 8 C; P < 0.0001). This Twist-dependent stabilization of cortical myosin II was even more dramatic in *arm-twiRNAi* embryos. In contrast to *armRNAi* embryos, where myosin II contracts into a stable cortical ring in each cell, myosin contractions in *arm-twiRNAi* embryos were pulsed, with myosin II disappearing from the cortex after coalescing (Fig. 8 D). Myosin II dynamics in *arm-twiRNAi* embryos were indistinguishable from *fog-t48-armRNAi* (*n* = 5 embryos), demonstrating that destabilization of cortical myosin II resulted directly from loss of function in the Twist pathway and not from lower Snail activity (Fig. 8 D). Given that contraction pulses are asynchronous in adjacent cells (Martin et al., 2009), we hypothesized that the failure to retain cortical myosin II between pulses would disrupt supracellular meshwork formation because only a subset of cells would have cortical myosin II at a given time. To test this, we segmented myosin-GFP images from control and *twiRNAi* embryos and measured the area of the largest myosin-GFP structure at each time point (Fig. 8 E). With our segmentation threshold, control embryos assembled large myosin II networks on the order of 200–300 μm², or the size of several cells (Fig. 8 F). However, *twiRNAi* embryos rarely exhibited myosin II networks larger than 50 μm², which corresponds to the apical area of an individual cell. We propose that Twist-dependent stabilization of apical myosin II fibers is required to form the supracellular actomyosin meshwork, which allows tension to be stably transmitted across the epithelium during ventral furrow formation.

Discussion

AJs integrate tensile force along the length of the ventral furrow

Recent studies have demonstrated the importance of actomyosin and AJs for individual cell shape changes and morphogenesis (Bertet et al., 2004; Dawes-Hoang et al., 2005; Franke et al., 2005; Blankenship et al., 2006; Gorfinkiel and Arias, 2007; Martin et al., 2009; Sawyer et al., 2009). However, less is known about the underlying mechanisms by which dynamic contractile forces are transmitted between cells of an epithelium and the resulting tissue mechanics. In this study, we examined the mechanics of ventral furrow formation both by lowering AJ levels and by ablating the apical actomyosin meshwork. Reducing AJ levels sensitized cell adhesion to stress, resulting in discrete, tissue-wide epithelial tears. We propose that tears in AJ-depleted embryos result from the loss of mechanical connections between cells when contractility exceeds the forces of adhesion. Interestingly, tears resulted from tissue separation along the a-p axis, which suggests that tension transmitted by AJs is mostly oriented along the length of the ventral furrow (Fig. 9 A). We confirmed this anisotropy in epithelial tension by showing that laser ablations in the ventral furrow also result in preferential
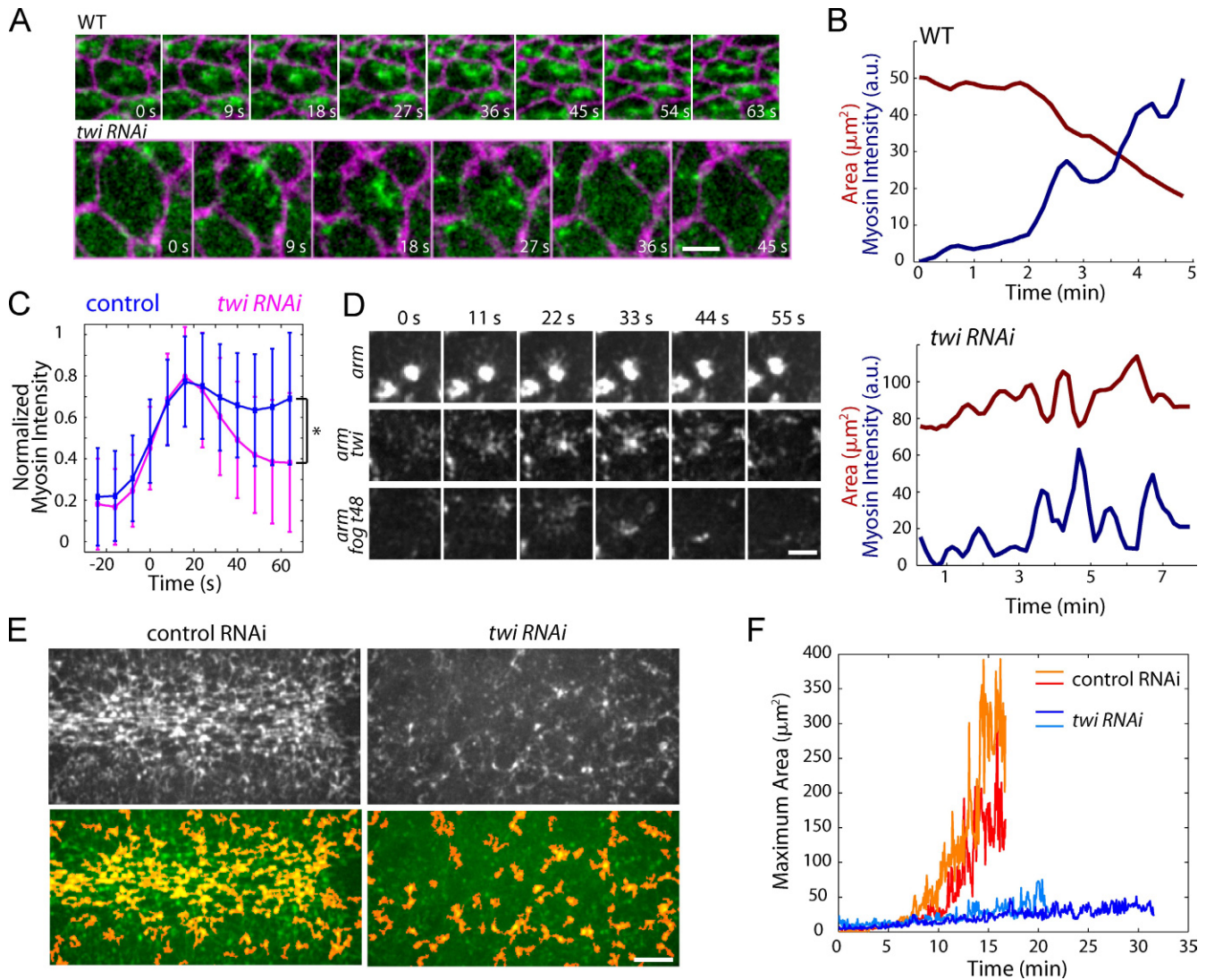
Figure 8. **Twist is required for myosin II stabilization and supracellular meshwork formation.** (A) Twist is required to stabilize apical myosin II fibers after contraction. Time-lapse images of myosin-GFP (green) and membrane-mCherry (purple). Bar, 5 µm. (B) Quantification of apical area (red) and myosin intensity (blue) in individual cells from wild-type and *twiRNAi* embryos. (C) Twist is required to maintain cortical myosin II after a contraction pulse. Normalized myosin intensity for individual contraction pulses was averaged. Data are means ± SD, which is indicated by the error bars (control: *n* = 329 pulses, 120 cells, two embryos; *twiRNAi*: *n* = 524 pulses, 106 cells, two embryos). (D) Twist is required to stabilize myosin II rings. Time-lapse images of myosin-GFP in embryos treated with *arm* dsRNA together with either *twi* or *fog/t48* dsRNA. Bar, 5 µm. (E) Myosin-GFP (top and bottom, green) in live control or *twiRNAi* embryos. Images were segmented using intensity and area thresholds to identify myosin II structures (bottom, red). Bar, 10 µm. (F) Twist is required to form the supracellular actomyosin meshwork. The area of the largest myosin II structure was quantified for each time point in videos of control-injected or *twiRNAi* embryos.

actomyosin retraction along the a-p axis. The global a-p retraction of the surrounding tissue after epithelial tearing suggests that the ventral furrow is a mechanically coherent epithelium, in which high levels of tensile force are integrated along the length of the furrow.

It is surprising that the vast majority of the epithelial tension generated by apical constriction is oriented along the length of the furrow, the axis with the least tissue movement. Indeed, one might have expected greater levels of tension along the v-l axis given that apical constriction is thought to pull lateral cells toward the ventral midline around the circumference of the embryo (Fig. 9 A). Future experiments are required to determine how anisotropic tension in the ventral furrow contributes to the bending and invagination of this epithelium.

Epithelial tension controls individual cell shape

Ventral furrow cells undergo polarized apical constriction, constricting predominantly in the v-l direction and remaining longer along the a-p axis (Sweeton et al., 1991). Because we failed to find a correlation between contraction pulses and cell anisotropy and because epithelial tension itself is anisotropic, we tested whether polarized apical constriction results from the mechanical constraints of the tissue. Indeed, epithelial tears allowed adjacent anisotropic cells to constrict isotropically, which suggests that ventral furrow cells attempt to constrict isotropically, but encounter greater resistance to constriction along the a-p axis (Fig. 9 B). During germ band extension, tension generated by supracellular actomyosin cables influences myosin

Figure 9. Causes and consequences of contractile force integration. (A) Distribution of apical tensile forces that accompany ventral furrow formation. Black arrows indicate the movement of lateral cells toward the ventral midline. Red arrows indicate epithelial tension, which is predominantly directed along the length of the furrow (a-p axis). (B) Tissue-level forces influence individual cell shape changes. Ventral furrow cells attempt to constrict isotropically (black arrows), but a-p tension (red arrows) resists constriction in this direction, resulting in anisotropic constriction. (C) Model for how contractile forces are integrated to generate epithelial tension in the ventral furrow. In wild-type embryos, pulses of actin (red) and myosin II (green) contraction constrict cell apices, and actomyosin fibers that remain on the apical surface between pulses maintain cortical tension (black arrows above cells), thus stabilizing cell shape. Actomyosin fibers linked by spot AJs (blue) form a supracellular meshwork that allows forces to be stably transmitted between cells, generating global epithelial tension (red arrows). In the absence of Twist, cells lack actomyosin fibers between contractions and fail to assemble a supracellular actomyosin meshwork. Thus, contraction pulses in cells stretch their immediate neighbors, and tension fails to be propagated across the epithelium.
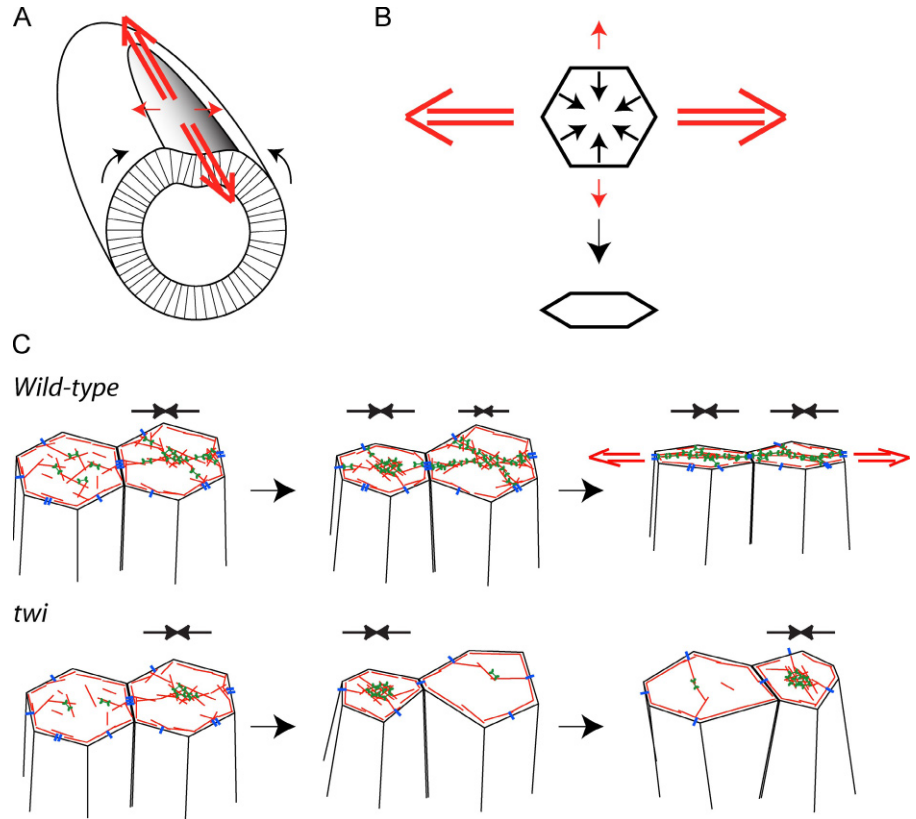
II assembly and dynamics within these cables (Fernandez-Gonzalez et al., 2009). Tension also appears to modulate actomyosin organization in the ventral furrow because epithelial tears resulted in unrestrained myosin II contraction into ring-like structures, as opposed to formation of a fibrous meshwork. Thus, the coupling of cellular contractile meshworks generates tension that feeds back to regulate both cytoskeletal organization/dynamics and cell shape. These results illustrate how the interplay between cell- and tissue-level forces influences cell shape change during morphogenesis.

Spot AJs transmit tensile forces oriented perpendicular to cell interfaces
Epithelial tension observed during ventral furrow formation likely resulted from contractile forces generated by apical actomyosin meshworks. We found that cellular actomyosin fibers were coupled end-to-end at spot AJs to form supracellular fibers and a tissue-wide meshwork. Disruption of AJs caused an imbalance of forces across the plasma membrane, resulting in membrane tethers. This supports a model in which tensile forces are integrated through discrete AJ anchors that link actomyosin networks in adjacent cells (Fig. 9 C). Supracellular actomyosin cables that transmit tension parallel to cell interfaces have been observed during germ band extension, dorsal closure, and compartment boundary formation (Rauzi et al., 2008; Rodriguez-Diaz et al., 2008; Fernandez-Gonzalez et al., 2009; Landsberg et al., 2009). However, in the ventral furrow, supracellular actomyosin fibers are mostly oriented perpendicular to cell interfaces (Fig. 9 C). This orientation is similar to that of actin in forming cultured epithelia, where radial actin fibers terminate in spot

junctions and form supracellular actin meshworks across the apical surface of epithelia (Yonemura et al., 1995; Adams et al., 1996; Vaezi et al., 2002). Furthermore, actin meshworks consisting of radial actin fibers emanating from central actin spots are also observed in *Xenopus* cells undergoing convergence and extension (Skoglund et al., 2008; Rolo et al., 2009). Actomyosin organization as a two-dimensional branched meshwork could represent a different mechanical paradigm for epithelial morphogenesis that enables cells to form a mechanically coherent sheet in which tensile forces are not restricted to cell interfaces, but bridge the surface of cells across the entire tissue.

Pulsatile and stable contractile networks cooperate to change cell shape and transmit tension across the tissue
Knockdown of the transcription factor Twist using RNAi separates the activities of pulsatile actomyosin contraction and cell shape stabilization between contractions (Martin et al., 2009). Pulses of actomyosin contraction continued to occur in both *twiRNAi* and *arm-twiRNAi* embryos. In *arm-twiRNAi* embryos, pulsed contractions disrupted cell–cell adhesion and formed membrane tethers, which suggests that pulsed contractions generate cellular tension that can separate the actomyosin network from AJs. A recent study of amnioserosa apical constriction proposed that contraction pulses are activated by mechanical interactions (i.e., stretching) between cells (Solon et al., 2009). However, in ventral furrow cells, pulsatile actomyosin contractions occurred even after cells lost adhesion, which suggests that pulsed contractions are fundamentally cell autonomous, possibly resulting from dynamic behaviors of cytoskeletal networks

(Munro et al., 2004; Paluch et al., 2005). Importantly, our data also showed that pulsed contractions were insufficient to generate epithelial tears. Thus, an additional mechanism is required to translate pulsatile contractile forces and cell shape changes into tissue-wide epithelial tension.

Twist-mediated stabilization is critical to transmit cellular forces to the tissue level. We show here that Twist was required for apical myosin II fibers to remain on the apical cortex between contraction pulses. These actomyosin fibers bridging the apical cortex likely stabilize the cell apex, preventing previously observed stretching events that would dissipate force transmission across the tissue (Martin et al., 2009). Furthermore, Twist-dependent myosin II stabilization allowed the formation of the supracellular actomyosin meshwork, which was critical for generating tissue-wide tension. We propose that this actomyosin meshwork results in a mechanically integrated tissue, allowing propagation of both pulsatile and stable tensile forces (Fig. 9 C). Thus, while pulsed contractions generate dramatic changes in individual cell shape, stabilizing tension produced by the supracellular actomyosin meshwork transmits these contractile forces to the tissue level, generating epithelial tension.

Pulsatile and stable contractile forces also cooperate to contract the amnioserosa during dorsal closure (Solon et al., 2009). During dorsal closure, amnioserosa contraction is stabilized by actomyosin cable assembly in the surrounding epidermis. However, in the ventral furrow, the machinery responsible for pulsation and stabilization are both present in the mesoderm. Future studies are needed to determine how actomyosin networks with unique properties are coordinated within the same cell. Interestingly, Twist is thought to activate G protein–coupled receptor signaling, which activates stress fiber formation in cultured cells (Buhl et al., 1995; Lin et al., 2005). Thus, Twist possibly induces actomyosin fiber assembly independently of pulsed contractions. Alternatively, pulsed contractions could bundle actomyosin meshworks to form fibers that become stabilized by Twist activity. Regardless of these different models, the cooperation of pulsatile and stable networks in morphogenetic events as diverse as epithelial invagination and sheet migration suggests that coordinated pulsation and stabilization represents a conserved mode of tissue morphogenesis.

Materials and methods

Fly stocks and genetics
The following stocks containing fluorescent fusion proteins were used: Spider-GFP (95–1) and Resille-GFP (117–2) (Morin et al., 2001), membrane-mCherry (this paper), myosin-GFP (sqh-GFP; Royou et al., 2002), and myosin-mCherry (sqh-mCherry; Martin et al., 2009). To examine cell shape in embryos devoid of a-p polarity, we used the stock w; Resille-GFP; bicoid^{E1} nanos^{L7} torso-like^{146}/TM3; Sb. We analyzed embryos from mothers that were homozygous for bicoid^{E1} nanos^{L7} torso-like^{146}. To generate arm$^{M/Z}$ mutants, we created arm^{043A01} germ-line clones using the FLP-DFS system (Chou and Perrimon, 1992). We visualized myosin II in arm$^{M/Z}$ mutants by generating a stock that was arm^{043A01} FRT101/FM7; sqh-GFP. We crossed females of this genotype to w ovo^D FRT101/Y; flp-138 males to obtain arm^{043A01} FRT101/w ovo^D FRT101; flp-138/+ females. These females were heat shocked as larvae for 2 h at 37°C each day to induce mitotic recombination in the germ line. We imaged embryos from the following cross: arm^{043A01} FRT101/w ovo^D FRT101; flp-138/+ females x FM7/+; flp-138/+ males. Half of these embryos showed loss of cell–cell adhesion, which is consistent with half being rescued zygotically.

Construction of membrane-mCherry
A membrane-mCherry marker was created by fusing the N-terminal 20 amino acids of the rat Gap43 gene, which contains a myristoylation sequence, to mCherry. This membrane-mCherry fusion was cloned into a pBluescript vector containing the sqh promoter and 3′ untranslated region (Martin et al., 2009). The 3-kilobase KpnI/XbaI sqh5′-membrane::mCherry-sqh3′ fragment was then inserted into a transformation vector containing the attB site (pTiger, courtesy of S. Ferguson, State University of New York at Fredonia, Fredonia, NY). The resulting construct was sent to Genetic Services, Inc., for integration into the attP2 site using the phiC31 integrase system (Groth et al., 2004).

Live cell imaging
To prepare embryos for live imaging, embryos were dechorionated with 50% bleach, washed with water, and mounted ventral side up on a slide covered with embryo glue (Scotch tape resuspended in heptane) between two No. 1.5 coverslip spacers. A coverslip was placed over the embryo and Halocarbon 27 oil was added to the resulting chamber. The spacers prevented the overlying coverslip from contacting the ventral surface of the embryo such that the embryo was not compressed. Embryos imaged under these conditions developed normally and subsequently hatched, demonstrating that our imaging conditions had minimal impact on development. All imaging was performed in Halocarbon 27 oil at room temperature (~23°C).

Spider-GFP, Resille-GFP, sqh-mCherry;Spider-GFP, and sqh-GFP; membrane-mCherry videos were obtained with a confocal microscope (SP5; Leica), a 63×/1.3 NA glycerine-immersion objective (Leica), an argon ion laser, and a 561-nm diode laser. Images were acquired using a pinhole setting from 1–2 airy units. For multichannel imaging, we set the excitation bandpass to 495–550 nm to detect GFP and 578–650 nm to detect mCherry. sqh-GFP single-channel videos were obtained using the aforementioned imaging system or with a spinning disk confocal microscope (Ultraview; PerkinElmer) controlled with Volocity Acquisition software (Improvision), a 60×/1.4 NA oil-immersion objective (Nikon), an argon/krypton laser, and an electron-multiplying charge-coupled device camera (C9100-13; Hamamatsu).

Laser ablation
Embryos were prepared for live imaging and were imaged using an Ultraview spinning disk confocal microscope equipped with a 63×/1.4 NA oil-immersion lens controlled with MetaMorph software (Universal Imaging). An N$_2$ Micropoint laser (Photonics Instruments) tuned to 365 nm was focused on sqh-GFP structures on the ventral surface of the embryo to ablate actomyosin structures. Point ablations were performed by ablating isotropic sqh-GFP spots with a point ~1 μm in diameter, which took ~670 ms. Line ablations were performed by making nine sequential point ablations to make a 20-μm incision, which took ~6.4 s. Z stacks were acquired immediately before and after ablation in order to measure displacement of myosin II structures upon release of tension.

Image processing and analysis
Images presented were processed using ImageJ (http://rsb.info.nih.gov/ij/) and Photoshop CS (Adobe Systems, Inc.). A Gaussian smoothing filter with a radius of one pixel was used to reduce noise in published images. Myosin II images presented in all figures are maximum intensity z projections of the apical ~5 μm of cells in the middle of the image. Because myosin II is almost entirely present on the apical surface of cells, these images represent a surface projection of the embryo. Images of cell outlines are z slices ~2 μm below the apical surface.

Image segmentation was performed using custom MATLAB (MathWorks) software. Raw images were bandpass filtered with effective cutoff wavelengths of ~1.4 μm (low pass) and ~16 μm (high pass). Images were then thresholded and skeletonized to reduce the width of the membranes to one pixel. Cells were then indexed and tracked based on the distance between cell centroids at subsequent time points. We manually removed cells with errors in the segmentation to ensure that all cells in the dataset were correctly identified. Aspect ratio and anisotropy were calculated by using the "regionprops" function in MATLAB to measure major axis length, minor axis length, and orientation for individual cells. We measured the intensity of cortical myosin II in individual cells using three-dimensional time-lapse videos that were ~5 μm in depth. To separate cortical myosin II structures from the diffuse cytoplasmic staining, we smoothed sqh-GFP images using a Gaussian smoothing filter with a three-pixel kernel size, σ = 0.5 pixels, and clipped intensity values three standard deviations above the mean. We then made maximum-intensity z projections of myosin II (averaging the two highest-intensity values) and integrated the intensity

of all the pixels in a given cell. Data for apical area, myosin intensity, and anisotropy were smoothed using a Gaussian smoothing filter (σ = 18–24 s, three time points) to remove noise.

Recoil of *sqh-GFP* structures after laser ablation was quantified using custom software in which myosin spots were hand selected and tracked from the pre-ablation frame to the post-ablation frame (Fernandez-Gonzalez et al., 2009).

To measure the continuity of the supracellular meshwork in control-injected and *twiRNAi* embryos, we thresholded maximum-intensity projections of *sqh-GFP* images using the mean pixel intensity as a cutoff. We then used the "bwmorph" function in MATLAB to identify connected objects and identified the largest object at each time point in a time-lapse video.

Embryo fixation and staining
To visualize cytoskeletal structures, embryos were fixed with 8% paraformaldehyde/heptane for 30 min, manually devitellinized, stained, and mounted in AquaPolymount (Polysciences, Inc.). Endogenous *sqh-GFP* fluorescence was used to visualize myosin II, and Alexa Fluor 568 phalloidin (Invitrogen) was used to visualize F-actin. *Drosophila* E-Cadherin (DCad2) was recognized using rat anti-DCad2 (Developmental Studies Hybridoma Bank) at a dilution of 1:50. Snail and neurotactin double stainings were performed in heat-fixed embryos using mouse anti-neurotactin (BP106; Developmental Studies Hybridoma Bank) and rabbit anti-Snail (a gift from M. Biggin, Lawrence Berkeley National Laboratory, Berkeley, CA) at dilutions of 1:100 and 1:1,000, respectively.

Scanning EM
Embryos were dechorionated with 50% bleach and fixed for 25 min at room temperature (23°C) with a 1:1 mixture of 25% glutaraldehyde in 0.1 M cacodylate buffer and heptane. The vitelline membrane was then manually removed with a needle, and embryos were dehydrated by gradually stepping up the concentration of ethanol (25%, 50%, 75%, 95%, and 100%). Embryos were then incubated for 10 min with a 1:1 mixture of ethanol and tetramethylsilane (TMS), and then with 100% TMS. The TMS was allowed to evaporate, and we transferred the embryos to the microscope stand and performed metal coating using a Desk II Sputterer (Denton Vacuum). Samples were imaged using a tabletop scanning EM (TM-1000; Hitachi).

RNAi
Primers for dsRNA were designed with E-RNAi (Arziman et al., 2005). Primers included the sequence of the T7 promoter (5′-TAATACGACTCAC-TATAGGGAGACCAC-3′) followed by the following recognition sequences: Arm-F, 5′-CCTGGTTACCATAGGCCAGA-3′; Arm-R, 5′-TGCCATCTCTA-ACAGCAACG-3′; ECad2-F, 5′-GAGAGGAGGCAACAGAAACG-3′; ECad2-R, 5′-GGACATACTCTCTAGCGGCG-3′; α-catenin-F, 5′-AAGCTG-CAAAATCGGGTAATGAAAA-3′, α-catenin-R, 5′-TCTAAGACTCGTTTGG-TGTAAATAC-3′; Fog-F, 5′-TGGTGACCAGTTCTCTTTCC-3′; Fog-R, 5′-TGTT-GCAGTTGCCGAAGT-3′; T48-F, 5′-CCGCCGGCTACTTGGA-3′; and T48-R, 5′-GAAAGAAGTCGATAAGCTGG-3′. For *twistRNAi*, *snaRNAi*, and control *CG3651RNAi*, we used the Twi01, Sna01, and control primer pairs (Martin et al., 2009). Primer pairs were used to amplify a PCR product from genomic DNA. PCR products were used in a transcription reaction with T7 polymerase using the MEGAscript transcription kit (Applied Biosystems). Annealing was performed by adding 10 mM EDTA, 0.1% SDS, and 0.1M NaCl to the reaction and incubating this mixture in a water bath heated to >90°C, which was allowed to cool for several hours. The dsRNA was purified by phenol/chloroform extraction and resuspended in injection buffer (5 mM KCl and 0.1 mM sodium phosphate, pH 7.0). Newly laid embryos were injected laterally and incubated for 2.5–3 h at room temperature (23°C) before imaging gastrulation. We injected AJ dsRNA at a concentration of ~1 mg/ml. However, tears in the myosin II network could be observed even after diluting dsRNA to a lower concentration. For most experiments, Arm dsRNA was used at 0.2 mg/ml. For double RNAi experiments, Arm dsRNA was used at 0.2 mg/ml, and Twist and Snail dsRNA was used at 2 mg/ml. For triple RNAi experiments, Arm dsRNA was used at 0.2 mg/ml, and Fog and T48 were used at 0.8 mg/ml and 0.65 mg/ml, respectively.

Online supplemental material
Fig. S1 shows that knockdown of E-cadherin, Arm, or α-catenin disrupts the myosin II network and results in membrane tethers. Fig. S2 shows myosin-GFP displacement as a function of time for the two types of laser ablation experiments shown in Fig. 3. Video 1 shows myosin-GFP in wild-type and *arm^{M/Z}* mutant embryos. Video 2 shows laser ablations in myosin-GFP embryos. Video 3 shows myosin-mCherry and membrane-GFP in an *armRNAi* embryo. Video 4 shows the contraction

of a myosin II fiber in an *arm^{M/Z}* mutant embryo. Video 5 shows the unrestrained myosin II contraction that occurs after tearing in an *armRNAi* embryo. Video 6 shows membrane tether formation in a membrane-GFP embryo. Video 7 shows myosin-GFP in a double RNAi control *arm-CG3651RNAi* embryo. Video 8 shows the suppression of tears and loss of cell–cell adhesion in a myosin-GFP *arm-snaRNAi* embryo. Video 9 shows that contraction pulses continue despite loss of cell–cell adhesion in a myosin-GFP *arm-twiRNAi* embryo. Video 10 shows the suppression of epithelial tears in a membrane-GFP *arm-twiRNAi* embryo. Online supplemental materials is available at http://www.jcb.org/cgi/content/full/jcb.200910099/DC1.

References

Adams, C.L., W.J. Nelson, and S.J. Smith. 1996. Quantitative analysis of cadherin-catenin-actin reorganization during development of cell–cell adhesion. *J. Cell Biol.* 135:1899–1911. doi:10.1083/jcb.135.6.1899

Arziman, Z., T. Horn, and M. Boutros. 2005. E-RNAi: a web application to design optimized RNAi constructs. *Nucleic Acids Res.* 33:W582–W588. doi:10.1093/nar/gki468

Bertet, C., L. Sulak, and T. Lecuit. 2004. Myosin-dependent junction remodelling controls planar cell intercalation and axis elongation. *Nature.* 429:667–671. doi:10.1038/nature02590

Blankenship, J.T., S.T. Backovic, J.S. Sanny, O. Weitz, and J.A. Zallen. 2006. Multicellular rosette formation links planar cell polarity to tissue morphogenesis. *Dev. Cell.* 11:459–470. doi:10.1016/j.devcel.2006.09.007

Buhl, A.M., N.L. Johnson, N. Dhanasekaran, and G.L. Johnson. 1995. G alpha 12 and G alpha 13 stimulate Rho-dependent stress fiber formation and focal adhesion assembly. *J. Biol. Chem.* 270:24631–24634. doi:10.1074/jbc.270.42.24631

Chou, T.B., and N. Perrimon. 1992. Use of a yeast site-specific recombinase to produce female germline chimeras in *Drosophila*. *Genetics.* 131:643–653.

Costa, M., E.T. Wilson, and E. Wieschaus. 1994. A putative cell signal encoded by the folded gastrulation gene coordinates cell shape changes during *Drosophila* gastrulation. *Cell.* 76:1075–1089. doi:10.1016/0092-8674(94)90384-0

Cox, R.T., C. Kirkpatrick, and M. Peifer. 1996. Armadillo is required for adherens junction assembly, cell polarity, and morphogenesis during *Drosophila* embryogenesis. *J. Cell Biol.* 134:133–148. doi:10.1083/jcb.134.1.133

Dawes-Hoang, R.E., K.M. Parmar, A.E. Christiansen, C.B. Phelps, A.H. Brand, and E.F. Wieschaus. 2005. Folded gastrulation, cell shape change and the control of myosin localization. *Development.* 132:4165–4178. doi:10.1242/dev.01938

Fernandez-Gonzalez, R., Sde.M. Simoes, J.C. Röper, S. Eaton, and J.A. Zallen. 2009. Myosin II dynamics are regulated by tension in intercalating cells. *Dev. Cell.* 17:736–743. doi:10.1016/j.devcel.2009.09.003

Franke, J.D., R.A. Montague, and D.P. Kiehart. 2005. Nonmuscle myosin II generates forces that transmit tension and drive contraction in multiple tissues during dorsal closure. *Curr. Biol.* 15:2208–2221. doi:10.1016/j.cub.2005.11.064

Gorfinkiel, N., and A.M. Arias. 2007. Requirements for adherens junction components in the interaction between epithelial tissues during dorsal closure in *Drosophila*. *J. Cell Sci.* 120:3289–3298. doi:10.1242/jcs.010850

Gorfinkiel, N., G.B. Blanchard, R.J. Adams, and A. Martinez Arias. 2009. Mechanical control of global cell behaviour during dorsal closure in *Drosophila*. *Development.* 136:1889–1898. doi:10.1242/dev.030866

Groth, A.C., M. Fish, R. Nusse, and M.P. Calos. 2004. Construction of transgenic *Drosophila* by using the site-specific integrase from phage phiC31. *Genetics.* 166:1775–1782. doi:10.1534/genetics.166.4.1775

Gumbiner, B.M. 2005. Regulation of cadherin-mediated adhesion in morphogenesis. *Nat. Rev. Mol. Cell Biol.* 6:622–634. doi:10.1038/nrm1699

Gustafson, T., and L. Wolpert. 1962. Cellular mechanisms in the morphogenesis of the sea urchin larva. Change in shape of cell sheets. *Exp. Cell Res.* 27:260–279. doi:10.1016/0014-4827(62)90229-X

Hardin, J., and R. Keller. 1988. The behaviour and function of bottle cells during gastrulation of *Xenopus laevis. Development.* 103:211–230.

Holtfreter, J. 1943. A study of the mechanics of gastrulation (part 1). *J. Exp. Zool.* 94:261–318. doi:10.1002/jez.1400940302

Hutson, M.S., Y. Tokutake, M.S. Chang, J.W. Bloor, S. Venakides, D.P. Kiehart, and G.S. Edwards. 2003. Forces for morphogenesis investigated with laser microsurgery and quantitative modeling. *Science.* 300:145–149. doi:10.1126/science.1079552

Kiehart, D.P., C.G. Galbraith, K.A. Edwards, W.L. Rickoll, and R.A. Montague. 2000. Multiple forces contribute to cell sheet morphogenesis for dorsal closure in *Drosophila. J. Cell Biol.* 149:471–490. doi:10.1083/jcb.149.2.471

Kölsch, V., T. Seher, G.J. Fernandez-Ballester, L. Serrano, and M. Leptin. 2007. Control of *Drosophila* gastrulation by apical localization of adherens junctions and RhoGEF2. *Science.* 315:384–386. doi:10.1126/science.1134833

Kosman, D., Y.T. Ip, M. Levine, and K. Arora. 1991. Establishment of the mesoderm-neuroectoderm boundary in the *Drosophila* embryo. *Science.* 254:118–122. doi:10.1126/science.1925551

Kumar, S., I.Z. Maxwell, A. Heisterkamp, T.R. Polte, T.P. Lele, M. Salanga, E. Mazur, and D.E. Ingber. 2006. Viscoelastic retraction of single living stress fibers and its impact on cell shape, cytoskeletal organization, and extracellular matrix mechanics. *Biophys. J.* 90:3762–3773. doi:10.1529/biophysj.105.071506

Landsberg, K.P., R. Farhadifar, J. Ranft, D. Umetsu, T.J. Widmann, T. Bittig, A. Said, F. Jülicher, and C. Dahmann. 2009. Increased cell bond tension governs cell sorting at the *Drosophila* anteroposterior compartment boundary. *Curr. Biol.* 19:1950–1955. doi:10.1016/j.cub.2009.10.021

Lecuit, T., and P.F. Lenne. 2007. Cell surface mechanics and the control of cell shape, tissue patterns and morphogenesis. *Nat. Rev. Mol. Cell Biol.* 8:633–644. doi:10.1038/nrm2222

Leptin, M. 1991. twist and snail as positive and negative regulators during *Drosophila* mesoderm development. *Genes Dev.* 5:1568–1576. doi:10.1101/gad.5.9.1568

Leptin, M. 2005. Gastrulation movements: the logic and the nuts and bolts. *Dev. Cell.* 8:305–320. doi:10.1016/j.devcel.2005.02.007

Leptin, M., and B. Grunewald. 1990. Cell shape changes during gastrulation in *Drosophila. Development.* 110:73–84.

Lin, F., D.S. Sepich, S. Chen, J. Topczewski, C. Yin, L. Solnica-Krezel, and H. Hamm. 2005. Essential roles of Galpha12/13 signaling in distinct cell behaviors driving zebrafish convergence and extension gastrulation movements. *J. Cell Biol.* 169:777–787. doi:10.1083/jcb.200501104

Martin, A.C., M. Kaschube, and E.F. Wieschaus. 2009. Pulsed contractions of an actin-myosin network drive apical constriction. *Nature.* 457:495–499. doi:10.1038/nature07522

Morin, X., R. Daneman, M. Zavortink, and W. Chia. 2001. A protein trap strategy to detect GFP-tagged proteins expressed from their endogenous loci in *Drosophila. Proc. Natl. Acad. Sci. USA.* 98:15050–15055. doi:10.1073/pnas.261408198

Munro, E., J. Nance, and J.R. Priess. 2004. Cortical flows powered by asymmetrical contraction transport PAR proteins to establish and maintain anterior-posterior polarity in the early *C. elegans* embryo. *Dev. Cell.* 7:413–424. doi:10.1016/j.devcel.2004.08.001

Odell, G.M., G. Oster, P. Alberch, and B. Burnside. 1981. The mechanical basis of morphogenesis. I. Epithelial folding and invagination. *Dev. Biol.* 85:446–462. doi:10.1016/0012-1606(81)90276-1

Paluch, E., M. Piel, J. Prost, M. Bornens, and C. Sykes. 2005. Cortical actomyosin breakage triggers shape oscillations in cells and cell fragments. *Biophys. J.* 89:724–733. doi:10.1529/biophysj.105.060590

Parks, S., and E. Wieschaus. 1991. The *Drosophila* gastrulation gene concertina encodes a G alpha-like protein. *Cell.* 64:447–458. doi:10.1016/0092-8674(91)90652-F

Peralta, X.G., Y. Toyama, M.S. Hutson, R. Montague, S. Venakides, D.P. Kiehart, and G.S. Edwards. 2007. Upregulation of forces and morphogenic asymmetries in dorsal closure during *Drosophila* development. *Biophys. J.* 92:2583–2596. doi:10.1529/biophysj.106.094110

Pouille, P.A., P. Ahmadi, A.C. Brunet, and E. Farge. 2009. Mechanical signals trigger Myosin II redistribution and mesoderm invagination in *Drosophila* embryos. *Sci. Signal.* 2:ra16. doi:10.1126/scisignal.2000098

Quintin, S., C. Gally, and M. Labouesse. 2008. Epithelial morphogenesis in embryos: asymmetries, motors and brakes. *Trends Genet.* 24:221–230. doi:10.1016/j.tig.2008.02.005

Rauzi, M., P. Verant, T. Lecuit, and P.F. Lenne. 2008. Nature and anisotropy of cortical forces orienting *Drosophila* tissue morphogenesis. *Nat. Cell Biol.* 10:1401–1410. doi:10.1038/ncb1798

Rodriguez-Diaz, A., Y. Toyama, D.L. Abravanel, J.M. Wiemann, A.R. Wells, U.S. Tulu, G.S. Edwards, and D.P. Kiehart. 2008. Actomyosin purse strings: renewable resources that make morphogenesis robust and resilient. *HFSP J.* 2:220–237. doi:10.2976/1.2955565

Rolo, A., P. Skoglund, and R. Keller. 2009. Morphogenetic movements driving neural tube closure in *Xenopus* require myosin IIB. *Dev. Biol.* 327:327–338. doi:10.1016/j.ydbio.2008.12.009

Royou, A., W. Sullivan, and R. Karess. 2002. Cortical recruitment of nonmuscle myosin II in early syncytial *Drosophila* embryos: its role in nuclear axial expansion and its regulation by Cdc2 activity. *J. Cell Biol.* 158:127–137. doi:10.1083/jcb.200203148

Sawyer, J.K., N.J. Harris, K.C. Slep, U. Gaul, and M. Peifer. 2009. The *Drosophila* afadin homologue Canoe regulates linkage of the actin cytoskeleton to adherens junctions during apical constriction. *J. Cell Biol.* 186:57–73. doi:10.1083/jcb.200904001

Shih, J., and R. Keller. 1992. Cell motility driving mediolateral intercalation in explants of *Xenopus laevis. Development.* 116:901–914.

Skoglund, P., A. Rolo, X. Chen, B.M. Gumbiner, and R. Keller. 2008. Convergence and extension at gastrulation require a myosin IIB-dependent cortical actin network. *Development.* 135:2435–2444. doi:10.1242/dev.014704

Sokac, A.M., and E. Wieschaus. 2008. Zygotically controlled F-actin establishes cortical compartments to stabilize furrows during *Drosophila* cellularization. *J. Cell Sci.* 121:1815–1824. doi:10.1242/jcs.025171

Solon, J., A. Kaya-Copur, J. Colombelli, and D. Brunner. 2009. Pulsed forces timed by a ratchet-like mechanism drive directed tissue movement during dorsal closure. *Cell.* 137:1331–1342. doi:10.1016/j.cell.2009.03.050

Sweeton, D., S. Parks, M. Costa, and E. Wieschaus. 1991. Gastrulation in *Drosophila*: the formation of the ventral furrow and posterior midgut invaginations. *Development.* 112:775–789.

Vaezi, A., C. Bauer, V. Vasioukhin, and E. Fuchs. 2002. Actin cable dynamics and Rho/Rock orchestrate a polarized cytoskeletal architecture in the early steps of assembling a stratified epithelium. *Dev. Cell.* 3:367–381. doi:10.1016/S1534-5807(02)00259-9

Yonemura, S., M. Itoh, A. Nagafuchi, and S. Tsukita. 1995. Cell-to-cell adherens junction formation and actin filament organization: similarities and differences between non-polarized fibroblasts and polarized epithelial cells. *J. Cell Sci.* 108:127–142.